The in-plane ferromagnetic ordering in half-metallic $CuCr_2Se_{4-x}Br_x$ (x=0.25) single crystal

Hui Han,[1,2] Lei Zhang,[1,*] Wei Tong,[1] Zhe Qu,[1]
Changjin Zhang,[1] Li Pi,[1,3] and Yuheng Zhang[1,3]

[1]*High Magnetic Field Laboratory, Chinese Academy of Sciences, Hefei 230031, China*

[2]*University of Science and Technology of China, Hefei 230026, China*

[3]*Hefei National Laboratory for Physical Sciences at the Microscale, University of Science and Technology of China, Hefei 230026, China*

(Dated: April 1, 2016)

chinaXiv:201712.01948v1

Abstract

The transport property of chalcogenide spinel $CuCr_2Se_4$ with an itinerant ferromagnetic ground state can be modulated by doping of bromine, where the half-metallic state can be realized around $x = 0.25$ in $CuCr_2Se_{4-x}Br_x$ system. In this work, the single crystal $CuCr_2Se_{4-x}Br_x$ (x =0.25) with the cleave surface (111) plane has been investigated by the electron paramagnetic resonance (EPR) spectroscopy. The EPR results show that the in-plane magnetization is strong while the out-of-plane one is weak, which indicate that the spins are ferromagnetic ordered within the (111) plane. In addition, the isothermal EPR spectra in the ferromagnetic phase display that the spin coupling strength (λ) and crystal field (Δ_{CF}) depend on the rotation angle φ as relation $\lambda/\Delta_{CF} \propto \cos\varphi$. Moreover, the peak-to-peak linewidth ΔH_{PP} increases linearly with the decrease of temperature, which suggests that the spin-orbit coupling is enhanced linearly with temperature cooling.

PACS numbers: 76.30.-v, 76.30.Fc, 75.50.Gg

Keywords: $CuCr_2Se_4$ single crystal; electron paramagnetic resonance; in-plane magnetization

*Corresponding author. Email: zhanglei@hmfl.ac.cn

chinaXiv:201712.01948v1

I. INTRODUCTION

Recently, chromium based chalcogenide spinel ACr_2Se_4 (A = Cu, Zn, Hg, Cr, Cd, *etc*) have been paid considerable attention due to exotic physical phenomena, such as Weyl semi-metal in $HgCr_2Se_4$ [1, 2], spin-orbit coupling in $CdCr_2Se_4$ [3], magnetoelectric effect or multiferocity in $ZnCr_2Se_4$ [4, 5]. The ferromagnetic selenide $CuCr_2Se_4$ is special due to the theoretical prediction of high spin-polarization and exhibition of significant magneto-optic Kerr rotation, which make it a perspective material for spintronics [6–12]. The $CuCr_2Se_4$, which holds an itinerant ferromagnetic ground state, displays the highest Curie temperature T_C of 430 K among spinel chalcogenides [13]. It is suggested that the ferrimagnetic hybridization between localized $3d^3$ electrons of Cr^{3+} ions and delocalized holes in Se $4p$ band results into a hole-mediated exchange [12]. This scenario has been confirmed by density functional calculations and magneto-optical study, where the appearance of a hybridization-induced hump-like band structure was observed at the Fermi energy only for the spin-up states [14, 15]. Moreover, the thermopower experiment has deomostated that the carriers are of p-type, which also supports the hole-mediated exchange mechanism [26].

It can be seen that the ferrimagnetic hybridization between Cr^{3+} and Se ions plays a key role in the transport and magnetic properties in $CuCr_2Se_4$ [12]. Therefore, the halogen doping in the Se-sites supplies an effective way to modulate transport and magnetic behaviors, such as the $CuCr_2Se_{4-x}Cl_x$ and $CuCr_2Se_{4-x}Br_x$ systems [17–19]. The $CuCr_2Se_{4-x}Br_x$ is well known for the dissipationless Anomalous Hall current, where the density of holes decreases from 7.2×10^{21} cm^{-1} for $x = 0$ to 1.9×10^{20} cm^{-1} for $x = 1.0$ [20, 21]. It is expected that the perfect half-metallic situation can be realized by tiny electron doping ($10 \sim 20$ % doping of Br as predicted by Butler *et al*) [6]. With the doping of bromine, the resistivity of this system evolves from metallic behavior for $x = 0$ to insulating state for $x = 1$, where $x = 0.25$ lies at the boundary [20]. Moreover, it has been demonstrated that the substitution of Br^- for Se^- ions in $CuCr_2Se_{4-x}Br_x$ system leads to the shift of the Kerr effect maximum energy near 1 eV to the higher energy region around $x = 0.25$ [22]. Therefore, $CuCr_2Se_{4-x}Br_x$ with $x = 0.25$ is close to a perfect half-metallic state.

In this work, the half-metallic $CuCr_2Se_{4-x}Br_x$ ($x = 0.25$) single crystal has been investigated by the electron paramagnetic resonance (EPR) spectroscopy. It is found that the spins are ferromagnetic ordered within the (111) plane, and the spin-orbit coupling strength

is enhanced almost linearly with the decrease of temperature.

II. EXPERIMENT

Single crystal $CuCr_2Se_{3.75}Br_{0.25}$ was prepared by the chemical vapor transportation (CVT) method [19, 20]. The phase purity, chemical compositions, and other physical properties were checked elsewhere [23]. The X-ray diffraction (XRD) pattern as shown in the upper inset of Fig. 1 (b) demonstrates that the naturally cleaved surface of the single crystal is (111) plane, in agreement with previous report [24]. The EPR measurement was carried out at selected temperatures using a Bruker EMX-plus model spectrometer operating at X-band frequencies ($\nu \approx 9.4$ GHz), and microwave power of 1 mW was used. The magnetic field was applied perpendicular and parallel to the naturally cleaved (111) plane respectively.

III. RESULTS AND DISCUSSION

Figure 1 (a) displays the temperature dependence of magnetization $[M(T)]$ (left axis) and reciprocal susceptibility $[\chi^{-1}(T) = (M/H)^{-1}]$ (right axis) for single crystal $CuCr_2Se_{3.75}Br_{0.25}$. The $M(T)$ curve shows typical magnetic ordering phase transition behavior. The phase transition temperature $T_C = 390$ K is determined from the minimum of dM/dT, as depicted in the inset of Fig. 1 (a). The $\chi^{-1}(T)$ curve almost exhibits a straight line above T_C, which indicates that it follows the Curie-Weiss (CW) law $\chi(T) = C/(T-\theta_{CW})$ ($C = N\mu_{eff}^2/3k_B$ is the Curie constant and θ_{CW} is the Curie-Weiss temperature). A linear fit to high temperature $\chi(T)$ yields that $C = 6.71$ emu K/ mole Oe and $\theta_{CW} = 390$ K. The effective moment is estimated to $\mu_{eff} = 3.66\ \mu_B/Cr^{3+}$. Considering that $\mu_{eff} = g_{eff}\sqrt{J(J+1)}$ (where g_{eff} is the Landé factor and J is the total angular momentum) [25, 26], it is estimated that $g_{eff} = 1.89$. Figure 1 (b) shows the rotation angle φ dependence of magnetization $[M(\varphi)]$ for $CuCr_2Se_{3.75}Br_{0.25}$ at 300 K in the ferromagnetic phase. The top inset of Fig. 1 (b) displays the XRD pattern for the cleavage surface, and the bottom inset sketches the measurement style. The $M(\varphi)$ curve indicates a good periodicity of the sample, with the maximum of the magnetization in (111) plane and the minimum out of (111) plane.

It is well known that the EPR spectroscopy is an effective technique to detect the miromagnetic interaction. Figure 2 shows the differential EPR spectra (dP/dH) for single crystal

chinaXiv:201712.01948v1

$CuCr_2Se_{3.75}Br_{0.25}$ at selected temperatures. As the cleave surface of the sample is (111) plane, the external magnetic field (H) is applied perpendicular and parallel to the (111) plane respectively. Figure 2 (a) shows the EPR spectra with H applied parallel to the (111) plane (in-plane). For the in-plane EPR spectra as shown in Fig. 2 (a), an EPR resonance signal is observed at ~ 3 kOe. The resonance signals are very weak above $T_C = 390$ K. With temperature decreasing, the EPR signal becomes strong from T_C to ~ 100 K. However, with further decrease of temperature, the EPR intensity becomes weaker from ~ 100 K to 2 K. Figure 2 (b) presents EPR spectra with H applied perpendicular to the (111) plane (out-of-plane). For the out-of-plane EPR spectra as shown in Fig. 2 (b), the resonance EPR signal is weaker than the in-plane one. With temperature decreasing, the out-of-plane EPR signals appear gradually above T_C. However, below T_C, it becomes weaker with the decrease of temperature. Meanwhile, a temperature-independent EPR signal appears at ~ 3 kOe below T_C, which may be caused by defects in the single crystal [27]. The phase transition temperature T_C determined by the EPR spectra is in agreement with that obtained by the $M(T)$ curve and the critical behaviors [23].

Figure 3 gives the rotation angle φ dependence of two-dimensional (2D) EPR spectra at $T = 380$ K in the ferromagnetic phase (the red color corresponds to the high intensity while the blue to low intensity). The top-left inset shows the measurement model, where the rotation angle φ is defined as the angle between H and the (111) plane. It can be seen that the EPR spectra present an apparent periodic behavior. The EPR intensity reaches the strongest at $\varphi = 0\,^\circ$ or $180\,^\circ$, while it is the weakest at $\varphi = 90\,^\circ$. In addition, the position of the EPR signal changes from lower field to higher field from $\varphi = 0\,^\circ$ to $90\,^\circ$, while it returns to lower field from $\varphi = 90\,^\circ$ to $180\,^\circ$. The top-right inset of Fig. 3 plots the g-factor as a function of φ, which is obtained as $g = h\nu/\mu_B H_r$ (where h is the Planck constant; ν is the used microwave freqency; H_r is the resonance field; μ_B is the Bohr magneton). The g-factor shows a periodic behavior, where the maximum of g-factor is 2.4 at $\varphi = 0°$ and $\varphi = 180°$, while it reaches the minimum at $\varphi = 90°$. As we know, the effective g-factor correlate with the crystal field (Δ_{CF}) and spin coupling strength with the environment (λ) as [28]:

$$g_{eff} = g_e + \frac{4\lambda}{\Delta_{CF}} \tag{1}$$

where g_e is the g-factor of a free electron. It is found that $\frac{4\lambda}{\Delta_{CF}}$ depends on φ as $\frac{4\lambda}{\Delta_{CF}} \propto \cos\varphi$. The fitting results give that $g_e = 2.003 \pm 0.004$, which is in agreement with the value

chinaXiv:201712.01948v1

of a free electron ($g = 2.0023$ with $S = 1/2$). These results indicate that the EPR signals are mainly produced by paramagnetic ions, which are modulated by the spin coupling and crystal field. The EPR results show that the magnetization is stronger within the (111) plane while it is weaker out of the (111) plane, which suggests a in-plane magnetic ordering in this system.

Figure 4 gives EPR parameters for the isothermal rotation spectra at $T = 380$ K in the ferromagnetic phase, including the φ dependence of H_r, EPR height, peak-to-peak linewidth ΔH_{pp}, and the double integrated intensity (I_{EPR}). All these parameters present periodic behaviors dependent on φ [as shown in Fig. 4 (a), (b) and (c)], except the I_{EPR} [as shown Fig. 4 (d)]. The H_r is defined as the magnetic field value at $dP/dH = 0$. In fact, the effective resonance field $H_r^{eff} = H_r + H_{int}$ (H_{int} is the internal field caused by the ferromagnetic ordering). According to the in-plane magnetic ordering scenario, when $\varphi = 0°$ (in-plane), the magnetization is strongest, which result into the strong H_{int}. Thus, the needful H_r is smaller. Contrarily, when $\varphi = 90°$ (out-of-plane), the H_{int} is weakest, the needful H_r is stronger. Therefore, the H_r is modulated periodically by the H_{int}. The EPR height as shown in Fig. 4 (b) shows the maximun at $\varphi = 0°$ while it reaches the minimum at $\varphi = 90°$, which also corresponds to the in-plane magnetic ordering in this system. As we know, the ΔH_{pp} directly reflects the spin coupling strength with the environment. The periodical change of ΔH_{pp} indicates that the spin coupling with the environment also changes periodically with φ. However, the tendency is opposite to the φ dependence of g-factor, which indicates that the determined factor of the isothermal g-factor is the crystal field rather than the spin coupling. The I_{EPR} as shown in Fig. 4 (d) is defined as the integrated area of the EPR spectrum, which usually corresponds to the number of paramagnetic ions participating into the resonance. The rare change of $I_{EPR}(\varphi)$ indicates that the isothermal number of paramagnetic ions does not change during the the rotation process.

From the results above, it can be seen that the in-plane magnetization is strong while the out-of-plane is weak, which suggest in-plane magnetic ordering in this system. In order to further investigate the magnetic interaction, the temperature dependence of EPR parameters are obtained. Due to the strong in-plane magnetization, the temperature dependence of in-plane EPR parameters are shown in Fig. 5. Figure 5 (a) gives the temperature dependence of H_r, where the right axis plots the g-factor. The H_r decreases with the decrease of temperature, corresponding to the increase of g-factor with the decrease of temperature. No

chinaXiv:201712.01948v1

abrupt changes can be observed at T_C for the temperature dependence of H_r and g-factor. The decrease of H_r may be due to the enhancement of the ferromagnetism with the decrease of temperature. An apparent change occurs to the temperature dependence of ΔH_{pp} at T_C, as shown in Fig. 5 (b). As we know, the ΔH_{pp} is corresponding to the spin coupling with the environment. With the decrease of temperature, ΔH_{pp} decreases sharply at $T_C = 390$ K. With further temperature cooling, ΔH_{pp} increases slightly with the decrease of temperature at a speed of 0.95 kOe/K. The abrupt decline of ΔH_{pp} indicates that drastic changes occur to the spin coupling with the surrounding environment due to the magnetic ordering transition. Above T_C in the paramagnetic phase, with temperature increasing, the thermal fluctuation of spins becomes stronger, which shorten the relaxation time τ. According to the relation $\Delta H_{pp} \propto 1/\tau$, ΔH_{pp} will be broadened with the increase of temperature in the paramagnetic regime [29]. Below T_C in the ferromagnetic phase, the increase of ΔH_{pp} with temperature decreasing may be due to the enhancement of spin coupling. As we know, there exists strong spin-orbit coupling in this system [30]. Therefore, the increase of ΔH_{pp} indicates the increase of the spin-orbit coupling with the decrease of temperature. It is noticed that the increase speed of ΔH_{pp} in single crystal sample is much smaller than that in the polycrystalline $CuCr_2Se_4$ (6.88 kOe/K) [31]. In a polycrystalline, ΔH_{pp} can be broadened due to the local dipolar field of pores and pits [32], which indicates that much crystal boundaries and defects affect significantly on the broaden of ΔH_{pp} in the polycrystalline. In the single crystal, the increase of ΔH_{pp} is mainly determined by the spin-orbit coupling. Figure 5 (c) gives the temperature dependence of the EPR height, which shows a corresponding change at T_C due to the ferromagnetic ordering. Figure 5 (d) shows the temperature dependence of I_{EPR}, which exhibits similar behavior as that in the polycrystal $CuCr_2Se_4$ [31]. Generally, the I_{EPR} is determined by the number of paramagnetic ions participating into the resonance. In the paramagnetic region, the I_{EPR} is proportional to $1/T$. Below T_C, the ferromagnetic phase becomes dominant in this system, leading to the dramatic decrease of the number of paramagnetic ions. The decreasing number of paramagnetic ions is responsible for the decrease of I_{EPR} in low temperature range [31].

chinaXiv:201712.01948v1

IV. CONCLUSION

In summary, single crystal $CuCr_2Se_{4-x}Br_x$ (x =0.25) with the cleave surface of (111) plane has been investigated by the EPR spectroscopy. The isothermal EPR results show that the in-plane magnetization is strong while out-of-plane one is weak, which indicate that the spins are ferromagnetic ordered within the (111) plane. In addition, the rotation angle φ dependence of isothermal EPR spectra shows that the spin coupling strength λ and crystal field Δ_{CF} depend on φ as $\lambda/\Delta_{CF} \propto \cos\varphi$. Moreover, it is found that the peak-to-peak linewidth ΔH_{PP} increases linearly with the decrease of temperature, which suggests that the spin-orbit coupling is enhanced linearly with temperature decreasing.

V. ACKNOWLEDGEMENTS

This work was supported by the State Key Project of Fundamental Research of China through Grant No. 2011CBA00111, the National Natural Science Foundation of China (Grant Nos. 11574322, U1332140, U1532267, 11574288, 11174291 and U1532153), the Foundation for Users with Potential of Hefei Science Center (CAS) through Grant No. 2015HSC-UP001.

chinaXiv:201712.01948v1

[1] G. Xu, H. Weng, Z. Wang, X. Dai, Z. Fang, Phys. Rev. Lett. **107** (2011) 186806.

[2] T. Guan, C. Lin, C. Yang, Y. Shi, C. Ren, Y. Li, H. Weng, X. Dai, Z. Fang, S. Yan, P. Xiong, Phys. Rev. Lett. **115** (2015) 087002.

[3] H. W. Lehmann, Phys. Rev. **163** (1967) 488.

[4] K. Siratori and E. Kita, J. Phys. Soc. Jpn. **48** (1980) 1443.

[5] H. Murakawa, Y. Onose, K. Ohgushi, S. Ishiwata, Y. Tokura, J. Phys. Soc. Jpn. **77** (2008) 043709.

[6] Y. Wang, A. Gupta, M. Chshiev, W. Butler, Appl. Phys. Lett. **92** (2008) 062507.

[7] Y. Wang, A. Gupta, M. Chshiev, W. Butler, Appl. Phys. Lett. **94** (2009) 062515.

[8] F. Ogata, T. Hamajima, T. Kambara, K. Gondaira, J. Phys. C: Solid State Phys. **15** (1982) 3483.

[9] H. Brandle, J. Schoenes, P. Wachter, F. Hulliger, W. Reim, Appl. Phys. Lett. **56** (1990) 2602.

chinaXiv:201712.01948v1

[10] V. G. Ivanov, M. N. Iliev, Y. H. A. Wang, A. Gupta, Phys. Rev. B **81** (2010) 224302.

[11] C. Pang, L. Gao, A. Chaturvedi, N. Z. Bao, K. Yanagisawa, L. M. Shen, A. Gupta, J. Mater. Chem. C **3** (2015) 12077.

[12] T. Saha-Dasgupta, M. Raychaudhury, D. Sarma, Phys. Rev. B **76** (2007) 054441.

[13] I. Nacatani, H. Nose, K. Masumoto, J. Phys. Chem. Solids **39** (1978) 743.

[14] V. Antonov, V. Antropov, B. Harmo, A. Yaresko, A. Perlov, Phys. Rev. B **59** (1998) 14552.

[15] S. Bordacs, I. Kezsmarki1, K. Ohgushi, Y. Tokura, New J. Phys. **12** (2010) 053039.

[16] I. Jendrzejewska, P. Zajdel, T. Gron, H. Duda, T. Mydlarz, J. Alloys Compd. **593** (2014) 158.

[17] A. Deb, M. Itou, V. Tsurkan, Y. Sakurai, Phys. Rev. B **75** (2007) 024413.

[18] K. Miyatani, K. Minematsu, Y. Wada, F. Okamoto, K. Kato, P. K. Baltzer, J. Phys. Chem. Solids **32** (1971) 1429.

[19] M. Liberati, J. R. Neulinger, R. V. Chopdekar, J. S. Bettinger, E. Arenholz, W. H. Butler, A. M. Stacy, Y. I. Idzerda, Y. Suzuki, J. Appl. Phys. **103** (2008) 07D711.

[20] W. L. Lee, S. Watauchi, V. L. Miller, R. J. Cava, N. P. Ong, Science **303** (2004) 1647.

[21] W. L. Lee, S. Watauchi, V. L. Miller, R. J. Cava, N. P. Ong, Phys. Rev. Lett. **93** (2004) 226601.

[22] R. Ivantsov, I. Edelman, S. Zharkov, D. Velikanov, D. Petrov, S. Ovchinnikov, C. Lin, O. Li, Y. Tseng, J. Alloys Compd. **650** (2015) 887.

[23] L. Zhang, J. Y. Fan, X. D. Zhu, W. Ning, Z. Qu, M. Ge, L Pi, Y. H. Zhang, Appl. Phys. A **113** (2013) 201.

[24] K. Borisov, J. Alaria, J. M. D. Coey, P. Stamenov, J. Appl. Phys. **115** (2014) 17C717.

[25] T. Gron, E. Tomaszewicz, M. Berkowski, B. Sawicki, P. Urbanowicz, J. Kusz, H. Duda, M. Oboz, Ceram. Int. **42** (2016) 4185.

[26] I. Jendrzejewska, T. Gron, E. Maciazek, H. Duda, M. Kubisztal, A. Slebarski, E. Pietrasik, M. Fijalkowski, J. Magn. Magn. Mater. **407** (2016) 122.

[27] L. Zhang, H. C. Lei, X. D. Zhu, W. Tong, C. J. Zhang, Y. H. Zhang, C. Petrovic, Phil. Mag. **93** (2013) 1132.

[28] J. Deisenhofer, S. Schaile, J. Teyssier, Z. Wang, M. Hemmida, H. Nidda, R. Eremina, M. Eremin, R. Viennois, E. Giannini, D. Marel, A. Loidl, Phys. Rev. B **86** (2012) 214417.

[29] S. Zhou, L. Shi, H. Yang, J. Zhao, Appl. Phys. Lett. **91** (2007) 172505.

[30] W. X. Feng, C. C. Liu, G. B. Liu, J. J. Zhou, Y. G. Yao, Comp. Mater. Sci. **112** (2016) 428.

[31] L. Zhang, W. Tong, J. Y. Fan, C. J. Zhang, R. W. Li, Y. H. Zhang, Eur. Phys. J. B **83** (2011) 325.

[32] M. Sparks, *Ferromagnetic Relaxation Theory*, McGraw Hill, (1960).

chinaXiv:201712.01948v1

chinaXiv:201712.01948v1

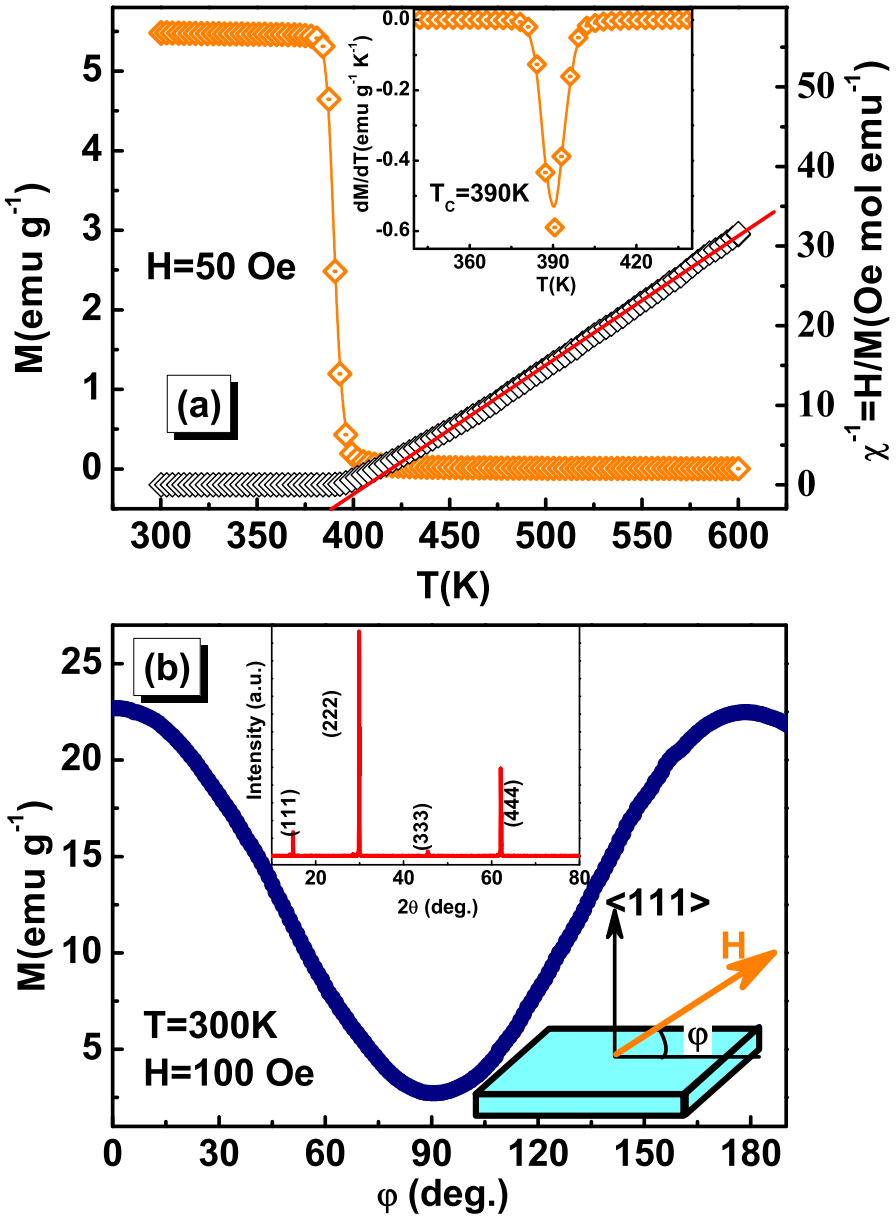

FIG. 1: (Color online) (a) The temperature dependence of magnetization $[M(T)]$ (left axis) and reciprocal susceptibility $[\chi(T)]$ (right axis) for $CuCr_2Se_{3.75}Br_{0.25}$ (the inset shows the dM/dT); (b) the rotation angle φ dependence of isothermal magnetization $[M(\varphi)]$ at 300 K (the top inset gives the XRD pattern for the cleavage surface; the bottom inset sketches the measurement style).

chinaXiv:201712.01948v1

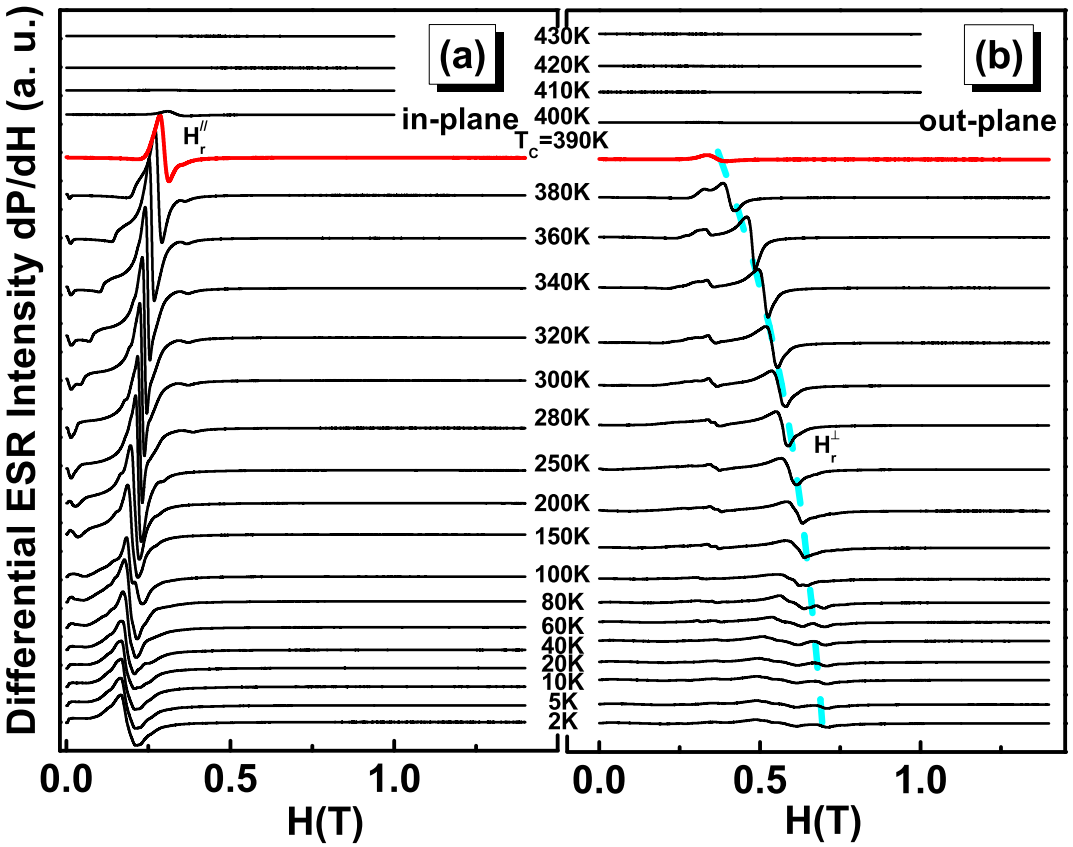

FIG. 2: (Color online) The differential EPR spectra (dP/dH) at selected temperatures for single crystal $CuCr_2Se_{3.75}Br_{0.25}$ with H applied (a) perpendicular (in-plane) and (b) parallel (out-of-plane) to the (111) plane.

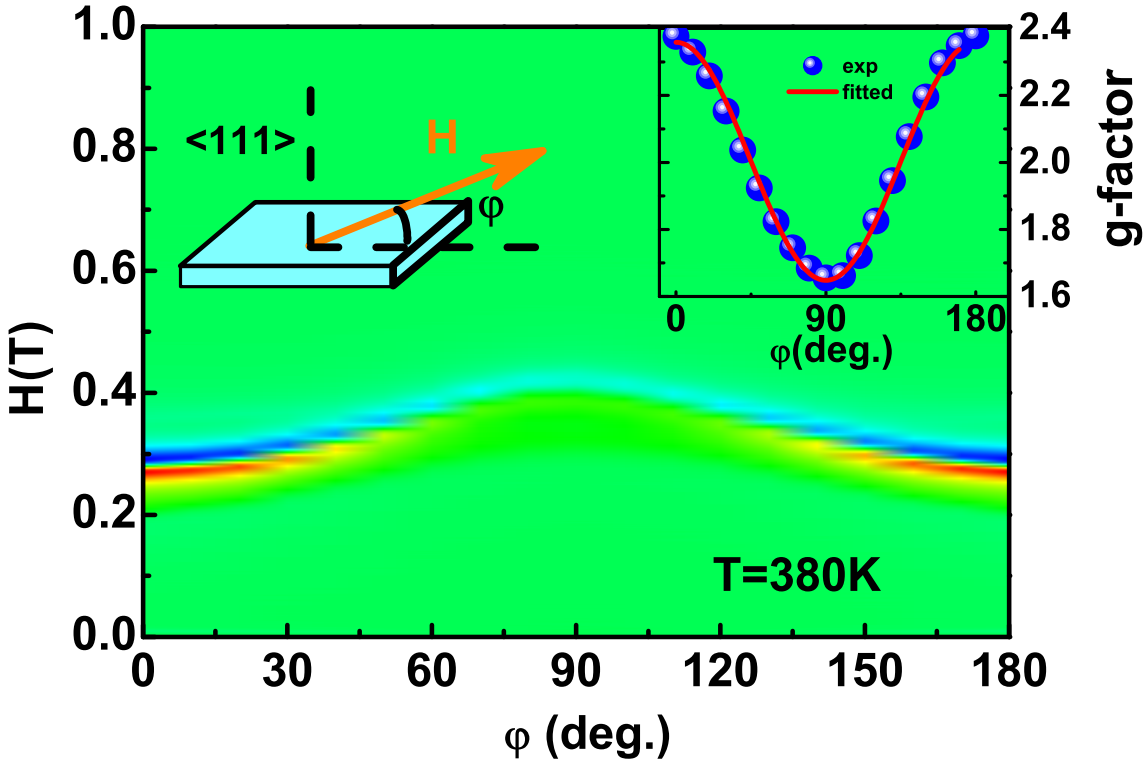

FIG. 3: (Color online) The two-dimensional (2D) isothermal EPR spectra at $T = 380$ K in the ferromagnetic phase (the red color corresponds to the high intensity while the blue to the low). The up-left inset shows the measurement style, while the top-right inset plots the g-factor as a function of the rotation angle φ (the solid curve is fitted).

chinaXiv:201712.01948v1

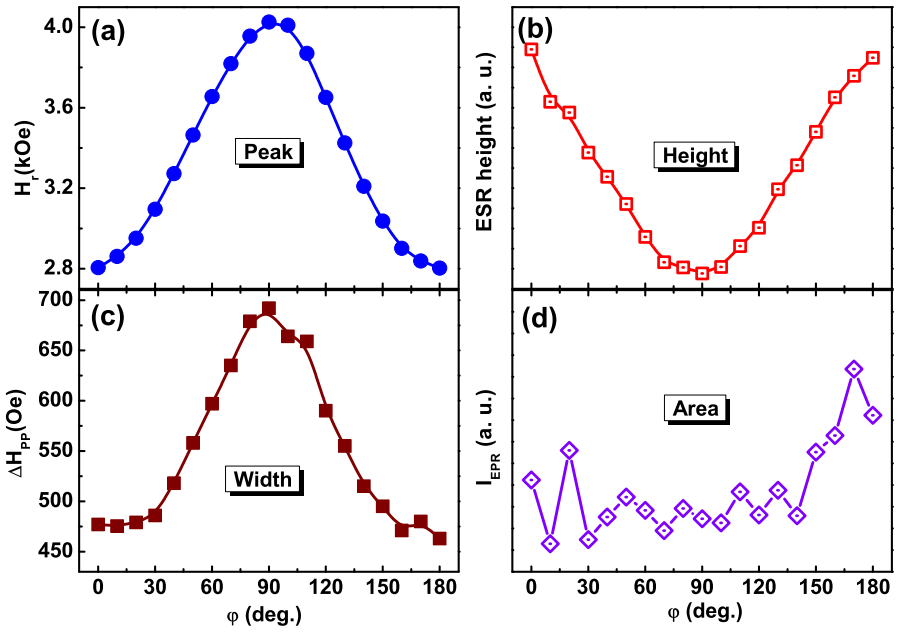

FIG. 4: (Color online) The EPR parameters for the isothermal rotation spectra at $T = 380$ K: (a) the resonance field H_r; (b) the EPR height; (c) the peak-to-peak linewidth ΔH_{pp}; (d) the double integrated intensity I_{EPR}.

chinaXiv:201712.01948v1

chinaXiv:201712.01948v1

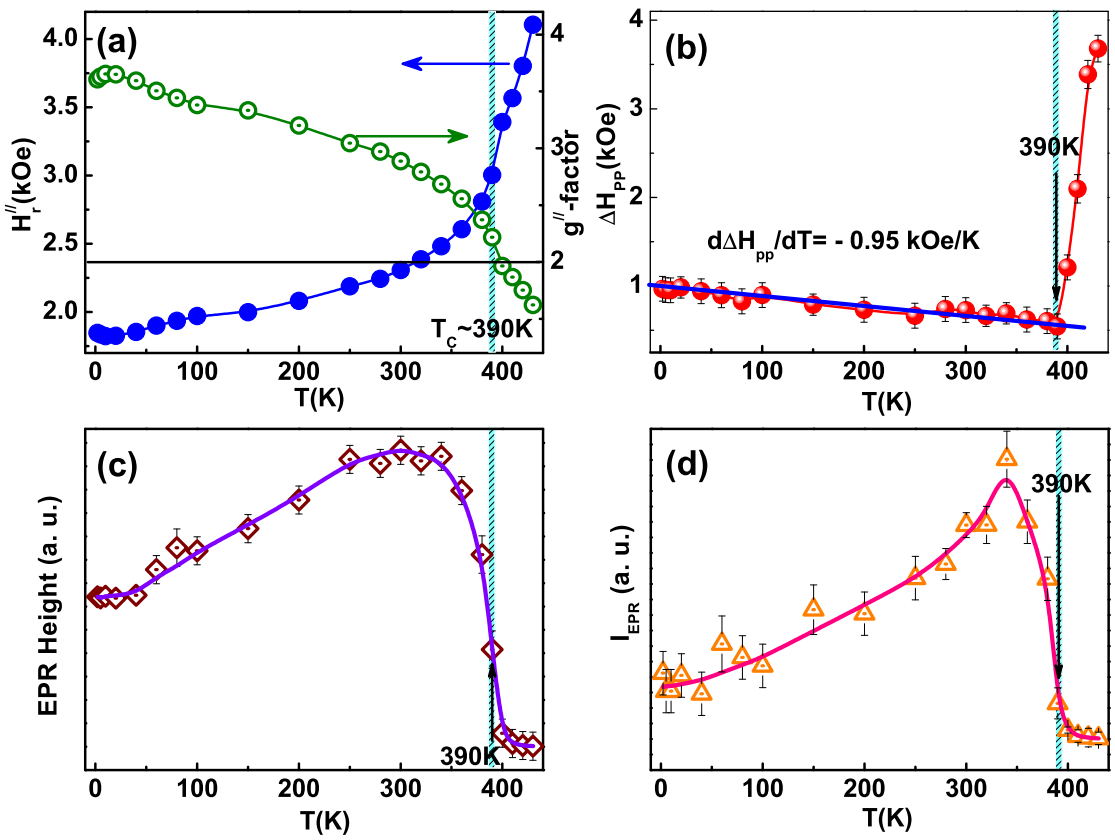

FIG. 5: (Color online) The temperature dependence of in-plane EPR parameters: (a) for the H_r and g-factor; (b) for the peak-to-peak linewidth ΔH_{pp}; (c) for the EPR height; (d) for the double integrated intensity I_{EPR}.